Commun. Comput. Phys.
doi: 10.4208/cicp.OA-2017-0203

Vol. **25**, No. 5, pp. 1446-1468
May 2019

Neutron Discrete Velocity Boltzmann Equation and its Finite Volume Lattice Boltzmann Scheme

Yahui Wang[1], Ming Xie[1,*] and Yu Ma[2,*]

[1] *School of Energy Science and Engineering, Harbin Institute of Technology, Harbin 150001, P.R. China.*
[2] *Sino-French Institute of Nuclear Engineering and Technology, Sun Yat-sen University, Zhuhai 519082, P.R. China.*

Received 23 September 2017; Accepted (in revised version) 22 January 2018

Abstract. Simulation of neutron transport process plays an important role in nuclear reactor computation and the numerical technique becomes the focus of nuclear reactor engineering. This paper provides a neutron finite volume lattice Boltzmann method (NFV-LBM) for solving the neutron discrete velocity Boltzmann equation (NDVBE), in which the NDVBE is deduced from the neutron transport equation (NTE) and the NFV-LBM is obtained by integrating the NDVBE. The macroscopic conservation equations recovered from the NDVBE via multi-scale expansion shows that the NDVBE has higher-order accuracy than diffusion theory, and the numerical solutions of neutron transport problems reveal the flexibility and applicability of NFV-LBM. This paper may provide some alternative perspectives for solving the NTE and some new ideas for researching the relationship between the NTE and other approximations.

AMS subject classifications: 60-08, 60J60, 62E17, 65C20

Key words: Neutron transport, neutron discrete velocity Boltzmann equation, neutron finite volume lattice Boltzmann, diffusion theory.

1 Introduction

Study of neutron particle transport in a scattering and absorbing medium represents a kernel in nuclear reactor physics and can be governed by the neutron transport equation (NTE), whose mono-energy scheme can be written as [1]

$$\begin{aligned}&\frac{1}{v}\frac{\partial\psi(\mathbf{r},\mathbf{\Omega},t)}{\partial t}+\mathbf{\Omega}\cdot\nabla\psi(\mathbf{r},\mathbf{\Omega},\ t)+\Sigma_t(\mathbf{r},t)\psi(\mathbf{r},\mathbf{\Omega},t)\\&=\int_{4\pi}\Sigma_s(\mathbf{r})f(\mathbf{r},\mathbf{\Omega}'\to\mathbf{\Omega})\psi(\mathbf{r},\mathbf{\Omega}',t)d\mathbf{\Omega}'+Q(\mathbf{r},\mathbf{\Omega},t),\end{aligned}\tag{1.1}$$

*Corresponding author. *Email addresses:* wangyahui@hit.edu.cn (Y. Wang), xieming@hit.edu.cn (M. Xie), mayu9@mail.sysu.edu.cn (Y. Ma)

where v is the speed of neutron particle; $\Omega = \boldsymbol{i}\mu + \boldsymbol{j}\eta + \boldsymbol{k}\xi = \boldsymbol{i}\sin\theta\cos\varphi + \boldsymbol{j}\sin\theta\sin\varphi + \boldsymbol{k}\cos\theta$ is the neutron transport direction with θ, φ represent the polar and azimuth angle, respectively; $\psi(\boldsymbol{r},\Omega,t)$ is neutron angular flux corresponding to position $\boldsymbol{r}$, angular direction Ω and time t; Σ_t and Σ_s are macroscopic total cross section and scattering cross section, respectively; $f(\boldsymbol{r},\Omega'\to\Omega)$ is the scattering phase function from direction Ω' to direction Ω; $Q(\boldsymbol{r},\Omega,t)$ is the neutron source.

Eq. (1.1) describes the mean neutron particle propagation within a given system [2], and has widely attracted the attention of various scientific communities, including neutron transport physics [1], nuclear reactor design [3], neutron capture therapies [4] and others [5, 6]. Due to its high dimensionality, simulation of this problem can be very difficult, especially for analytical methods. Thus, with the development of digital computer and numerical computing method, numerical techniques for solving this problem have received a substantial amount of interests from the research community.

In solving the neutron transport problem, a large number of techniques have been raised and developed based on the statistical approach, such as Monte Carlo method (MCM) [7–9], and deterministic techniques, including those of discrete-ordinates method (DOM, also be known as S_N) [10, 11], spherical harmonics method (P_N) [12], the method of characteristics (MOC) [13, 14] and finite different method (FDM) [15]. MCM is valuable as its high precision and capability of treating very complex configurations, but limited by its highly computational resource and stochastic statistical uncertainty [16, 17]. Thus, the deterministic methods, based on the solution of mathematical physics equations, have covered a wide scope of numerical methods and technologies. By using the DOM, the continuous solid angle domain can be discretized and the neutron angular flux is assumed constant within each direction, which leads to a series of discrete-ordinate NTEs [6]

$$\frac{1}{v}\frac{\partial\psi_\alpha(\boldsymbol{r},t)}{\partial t}+\Omega_\alpha\cdot\nabla\psi_\alpha(\boldsymbol{r},t)+\Sigma_t(\boldsymbol{r},t)\psi_\alpha(\boldsymbol{r},t)=S_{d,\alpha}(\boldsymbol{r},t)+Q_\alpha(\boldsymbol{r},t), \tag{1.2}$$

where the subscript α represents the index of neutron transport discrete direction and the neutron distribution function is defined as $\psi_\alpha(\boldsymbol{r},t)=\psi(\boldsymbol{r},\Omega,t)$; S_d is the scattering source term defined by

$$S_d(\boldsymbol{r},\Omega,t)=\Sigma_t(\boldsymbol{r},t)\sum_{\alpha'=1}^{M}\Delta\Omega_{\alpha'}\psi_{\alpha'}(\boldsymbol{r},t)f(\alpha,\alpha'). \tag{1.3}$$

Then, this series of NTEs can be solved by using conventional method such as MOC and FDM. It can be easily to find out that the number of computing equations is equal to the product of nodes number and directions number, which leads to the issue that when solving the multi-dimensional problem, the number of solving equations can easily exceed millions. Besides, the existing deterministic methods are relatively complicated for complex geometry. To improve these conditions, two types of thoughts may be considered: a novel technique for effectively resolving the NTE, and a further reduction for angular dependence.

In comparison, the lattice Boltzmann method (LBM) [18–20] may be an optional deterministic method with attractive advantages in solving hydrodynamics [21], such as simple construction, highly parallel efficiency and easy treatment of complex boundary [22]. Owing to these advantages, the LBM attracts a growing interest and gets a great development in many research fields, including fluid flow [23–26], heat and mass transfer [27–29], radiative heat transfer [30, 31], multi-phase flow [32], porous flow [33], thermal channel flow [34], complex micro flow [35, 36], magneto hydrodynamic [37] and phonon transport [38, 39]. Based on the lattice Boltzmann model presented by Ma et al. [30], Bindra et al. [40] extended the LBM to obtain the solution for the linear NTE and the solutions agree well with P_1 (the first-order spherical harmonic method) and S_2 (the DOM with 8 discrete directions) solutions. After that, some further researches for solving the neutron and radiative transport problems are reported based on this model [41, 42]. These work can be more accurate by using more lattice speed and more flexible by using unstructured mesh. When applying the multi-speed lattice Boltzmann model [43–45] or discrete Boltzmann model, the highly angular resolution of NTE can be ensured, and the number of different lattice speeds corresponds to different calculation accuracies. Besides, the unstructured mesh can be achieved by using the finite volume lattice Boltzmann method [46–49]. Moreover, the transient study is inadequate in previous work, which makes the research of strong transient processes not comprehensive. In addition, since the neutron transport process is described by a linear Boltzmann equation, a direct evolution of the angle-dependent neutron particle distribution function in LBM still remains an open challenge [30, 39]. To improve these conditions, our work presents a multi-speed neutron discrete velocity Boltzmann equation (NDVBE) and solve it by using neutron finite volume lattice Boltzmann method (NFV-LBM). The unstructured mesh (hexahedron mesh for 3D and quadrilateral mesh for 2D) is applied to adapt the complex geometry.

In simulating the large scale nuclear reactor engineering, researchers always simplify the neutron transport theory by applying the isotropic approximation and integrating the angular flux over angular space, which leads to the neutron diffusion theory [1]. To further study the relationship between NDVBE and neutron diffusion theory, we analyze them from the perspectives of mathematics and numerical calculation, including the recovery of diffusion theory from NDVBE via the lower-order multi-scale expansion, and the deviations between NFV-LBM and diffusion theory solutions.

The rest of this paper is organized as follows. In Section 2, the details of the NFV-LBM are introduced, including the NDVBE, its relationship to diffusion theory, the finite volume lattice Boltzmann scheme and the treatments of typical boundary conditions. In Section 3, numerical cases are simulated to verify the proposed NFV-LBM. Section 4 studied the deviations between NFV-LBM and diffusion theory solutions. The conclusions are drawn in Section 5.

2 Numerical theory

In this section, the NDVBE is deduced from the NTE and the neutron diffusion theory is recovered from NDVBE via the lower-order Chapman-Enskog expansion. After that,

the NFV-LBM is introduced by integrating the NDVBE over the control volume. The treatments of typical boundary conditions are listed at the rest of this section.

2.1 The neutron discrete velocity Boltzmann equation

In light of multi-speed lattice Boltzmann method, we tune the neutron transport directions along the discrete lattice directions (i.e., to modify the discrete direction vector $\mathbf{\Omega}_\alpha$ along the lattice speed $\mathbf{e}_\alpha$). The corresponding evolution equation, namely multi-speed NDVBE with the BGK approximation can be given as

$$\frac{\partial \psi_\alpha(\mathbf{r},t)}{\partial t}+\mathbf{e}_\alpha\cdot\nabla\psi_\alpha(\mathbf{r},t)=-\frac{\psi_\alpha(\mathbf{r},t)-\psi_\alpha^{eq}(\mathbf{r},t)}{\tau_c}+\Pi_\alpha(\psi), \tag{2.1}$$

where ψ_α^{eq} is the equilibrium neutron distribution function and $\mathbf{e}_\alpha=v\mathbf{\Omega}_\alpha$ is the lattice speed. τ_c is the relaxation time related to the particle speed and macroscopic total cross section. The first part of right hand side (RHS) is so called collision term, which stems from the consideration of inter-particle collision. However, when considering the neutron transport process, the inter-particle collision can be neglected, thus the collision term of Eq. (2.1) can be removed [40] and the Eq. (2.1) can be rewritten as

$$\frac{\partial \psi_\alpha(\mathbf{r},t)}{\partial t}+\mathbf{e}_\alpha\cdot\nabla\psi_\alpha(\mathbf{r},t)=\Pi_\alpha(\psi), \tag{2.2}$$

where $\Pi_\alpha(\psi)$ is the total source term corresponding to the neutron distribution function defined by

$$\Pi_\alpha(\psi)=v\Sigma_s\sum_{\alpha'=1}^{M}\Delta\mathbf{\Omega}_{\alpha'}\psi_{\alpha'}f(\alpha,\alpha')+vQ_\alpha-v\Sigma_t\psi_\alpha. \tag{2.3}$$

By defining different various lattice speeds, the transport equation of different accuracies can be achieved. The previous work [40] showed that when applying D1Q2, D2Q4 and D3Q6 lattices, the results will close to the diffusion theory. In the present work, in order to obtain the neutron transport precision, we adopt D1QM, D2QM and D3QM lattice, in which the number M is larger than previous work and will be discussed below.

To satisfy the neutron particle conservation, the scalar neutron flux can be obtained as [6]

$$\phi(\mathbf{r},t)=\sum_{\alpha=1}^{M}\psi_\alpha(\mathbf{r},t)\Delta\mathbf{\Omega}_\alpha. \tag{2.4}$$

By introducing a very small parameter K and defining three time scales, including collision time scale K^0, convective time scale K^{-1} and diffusion time scale K^{-2}, the continuous temporal and spatial scales can be expressed as

$$t_1=Kt,\quad t_2=K^2t, \tag{2.5}$$

$$\mathbf{r}_0=K\mathbf{r}. \tag{2.6}$$

With the above definitions, the temporal and spatial derivatives can be expanded as

$$\frac{\partial}{\partial t}=K\frac{\partial}{\partial t_1}+K^2\frac{\partial}{\partial t_2},\quad \frac{\partial}{\partial \mathbf{r}}=K\frac{\partial}{\partial \mathbf{r}_1}. \tag{2.7}$$

Similarly, by assuming that the distribution function and source term is near equilibrium, the discrete neutron distribution function and discrete source term can asymptotically expanded as [22]

$$\begin{aligned}&\psi_\alpha=\psi_\alpha^{eq}+K\psi_\alpha^{(1)}+K^2\psi_\alpha^{(2)}+\mathcal{O}\left(K^3\right),\\&Q_\alpha=Q_\alpha^{eq}+KQ_\alpha^{(1)}+\mathcal{O}\left(K^2\right),\\&\hat{Q}=\hat{Q}^{eq}+K\hat{Q}_\alpha^{(1)}+\mathcal{O}\left(K^2\right),\end{aligned} \tag{2.8}$$

where $\hat{Q}$ is the summation of angular source in each direction.

The conservation law of neutron particle distribution should be ensured by satisfying the following process

$$\begin{aligned}&\sum_{\alpha=1}^{M}\psi_\alpha^{eq}\Delta\mathbf{\Omega}_\alpha=\phi,\quad \sum_{\alpha=1}^{M}\mathbf{e}_\alpha\psi_\alpha^{eq}\Delta\mathbf{\Omega}_\alpha=v\mathbf{J},\quad \sum_{\alpha=1}^{M}Q_\alpha\Delta\mathbf{\Omega}_\alpha=\hat{Q}_\alpha,\\&\sum_{\alpha}^{M}\psi_\alpha^{(n)}\Delta\mathbf{\Omega}_\alpha=0,\quad \sum_{\alpha}^{M}\mathbf{e}_\alpha\psi_\alpha^{(n)}\Delta\mathbf{\Omega}_\alpha=0,\quad \sum_{\alpha}^{M}\mathbf{e}_\alpha\mathbf{e}_\alpha\psi_\alpha^{(n)}\Delta\mathbf{\Omega}_\alpha=0,\quad n\geq 1,\end{aligned} \tag{2.9}$$

where $\mathbf{J}$ is the neutron current flux.

Applying Eqs. (2.7) and (2.8) to Eq. (2.2), the multi-scale NDVBE can be written as

$$\begin{aligned}&\left(K\frac{\partial}{\partial t_1}+K^2\frac{\partial}{\partial t_2}\right)\left(\psi_\alpha^{eq}+K\psi_\alpha^{(1)}+K^2\psi_\alpha^{(2)}\right)\\&\quad+K\left(\mathbf{e}_\alpha\cdot\nabla_1\right)\left(\psi_\alpha^{eq}+K\psi_\alpha^{(1)}+K^2\psi_\alpha^{(2)}\right)+v\Sigma_t\left(\psi_\alpha^{eq}+K\psi_\alpha^{(1)}+K^2\psi_\alpha^{(2)}\right)\\&=v\Sigma_s\sum_{\alpha'=1}^{M}\left(\psi_{\alpha'}^{eq}+K\psi_{\alpha'}^{(1)}+K^2\psi_{\alpha'}^{(2)}\right)\Delta\mathbf{\Omega}_{\alpha'}f\left(\alpha,\alpha'\right)+v\left(Q_\alpha^{eq}+KQ_\alpha^{(1)}\right).\end{aligned} \tag{2.10}$$

Equating the parameters in the same order of K, one can obtain the subsequent orders of magnitude on K^0, K^1 and K^2, respectively

$$\Sigma_t\psi_\alpha^{eq}=\Sigma_s\sum_{\alpha'=1}^{M}\psi_{\alpha'}^{eq}\Delta\mathbf{\Omega}_{\alpha'}f\left(\alpha,\alpha'\right)+Q_\alpha^{eq}, \tag{2.11}$$

$$\frac{\partial\psi_\alpha^{eq}}{\partial t_1}+\left(\mathbf{e}_\alpha\cdot\nabla_1\right)\psi_\alpha^{eq}+v\Sigma_t\psi_\alpha^{(1)}=v\Sigma_s\sum_{\alpha'=1}^{M}\psi_{\alpha'}^{(1)}\Delta\mathbf{\Omega}_{\alpha'}f\left(\alpha,\alpha'\right)+vQ_\alpha^{(1)}, \tag{2.12}$$

$$\frac{\partial\psi_\alpha^{(1)}}{\partial t_1}+\frac{\partial\psi_\alpha^{eq}}{\partial t_2}+\left(\mathbf{e}_\alpha\cdot\nabla_1\right)\psi_\alpha^{(1)}+v\Sigma_t\psi_\alpha^{(2)}=v\Sigma_s\sum_{\alpha'=1}^{M}\psi_{\alpha'}^{(2)}\Delta\mathbf{\Omega}_{\alpha'}f\left(\alpha,\alpha'\right). \tag{2.13}$$

It is clearly that in equilibrium state, the attenuation term equals to the summation of scattering source and external source. Calculating the zeroth-order and first-order moments of Eq. (2.11), one obtains:

$$\Sigma_t\phi=\Sigma_s\sum_{\alpha=1}^{M}\Delta\mathbf{\Omega}_\alpha\sum_{\alpha'=1}^{M}\psi_{\alpha'}^{eq}f\left(\alpha,\alpha'\right)\Delta\mathbf{\Omega}_{\alpha'}+\hat{Q}^{eq}, \tag{2.14}$$

$$\Sigma_t v^2\mathbf{J}=v\Sigma_s\sum_{\alpha=1}^{M}\mathbf{e}_\alpha\Delta\mathbf{\Omega}_\alpha\sum_{\alpha'=1}^{M}\psi_{\alpha'}^{eq}f\left(\alpha,\alpha'\right)\Delta\mathbf{\Omega}_{\alpha'}+v\sum_{\alpha=1}^{M}\mathbf{e}_\alpha Q_\alpha^{eq}\Delta\mathbf{\Omega}_\alpha. \tag{2.15}$$

Similarly, calculate the zeroth- and first-order moments for Eq. (2.12) and (2.13), one obtains:

$$\frac{1}{v}\frac{\partial}{\partial t_1}\phi+\nabla_1\cdot\mathbf{J}=\Sigma_s\sum_{\alpha=1}^{M}\Delta\mathbf{\Omega}_\alpha\sum_{\alpha'=1}^{M}\psi_{\alpha'}^{(1)}f\left(\alpha,\alpha'\right)\Delta\mathbf{\Omega}_{\alpha'}+\hat{Q}^{(1)}, \tag{2.16}$$

$$\begin{aligned}&\frac{\partial}{\partial t_1}v\mathbf{J}+\nabla_1\cdot\sum_{\alpha=1}^{M}\mathbf{e}_\alpha\mathbf{e}_\alpha\psi_\alpha^{eq}\Delta\mathbf{\Omega}_\alpha\\&\quad=v\Sigma_s\sum_{\alpha=1}^{M}\mathbf{e}_\alpha\Delta\mathbf{\Omega}_\alpha\sum_{\alpha'=1}^{M}\psi_{\alpha'}^{(1)}f\left(\alpha,\alpha'\right)\Delta\mathbf{\Omega}_{\alpha'}+v\sum_{\alpha=1}^{M}\mathbf{e}_\alpha Q_\alpha^{(1)}\Delta\mathbf{\Omega}_\alpha,\end{aligned} \tag{2.17}$$

and

$$\frac{1}{v}\frac{\partial}{\partial t_2}\phi=\Sigma_s\sum_{\alpha=1}^{M}\Delta\mathbf{\Omega}_\alpha\sum_{\alpha'=1}^{M}\psi_{\alpha'}^{(2)}f\left(\alpha,\alpha'\right)\Delta\mathbf{\Omega}_{\alpha'}, \tag{2.18}$$

$$\frac{\partial}{\partial t_2}v\mathbf{J}=v\Sigma_s\sum_{\alpha=1}^{M}\mathbf{e}_\alpha\Delta\mathbf{\Omega}_\alpha\sum_{\alpha'=1}^{M}\psi_{\alpha'}^{(2)}f\left(\alpha,\alpha'\right)\Delta\mathbf{\Omega}_{\alpha'}. \tag{2.19}$$

Taking (2.14) + $K\times$ (2.16) + $K^2\times$ (2.18) and (2.15) + $K\times$ (2.17) + $K^2\times$ (2.19), one obtains the macroscopic equations:

$$\frac{1}{v}\frac{\partial}{\partial t}\phi+\nabla\cdot\mathbf{J}+\Sigma_t\phi=\Sigma_s\sum_{\alpha=1}^{M}\Delta\mathbf{\Omega}_\alpha\sum_{\alpha'=1}^{M}\psi_{\alpha'}f\left(\alpha,\alpha'\right)\Delta\mathbf{\Omega}_{\alpha'}+\hat{Q}_\alpha, \tag{2.20}$$

$$\begin{aligned}&\frac{\partial}{\partial t}v\mathbf{J}+\nabla\cdot\sum_{\alpha=1}^{M}\mathbf{e}_\alpha\mathbf{e}_\alpha\psi_\alpha^{eq}\Delta\mathbf{\Omega}_\alpha+\Sigma_t v^2\mathbf{J}\\&\quad=v\Sigma_s\sum_{\alpha=1}^{M}\mathbf{e}_\alpha\Delta\mathbf{\Omega}_\alpha\sum_{\alpha'=1}^{M}\psi_{\alpha'}f\left(\alpha,\alpha'\right)\Delta\mathbf{\Omega}_{\alpha'}+\sum_{\alpha=1}^{M}\mathbf{e}_\alpha Q_\alpha^{eq}\Delta\mathbf{\Omega}_\alpha.\end{aligned} \tag{2.21}$$

Then, we apply some conditions to simplify these equations:

1. We assume that the external source is isotropic, which is reasonable since the fusion source in nuclear reactor is nearly isotropic. Thus the first-order moment of external source is equal to zero:
$$\sum_{\alpha=1}^{M} \mathbf{e}_\alpha Q_\alpha^{eq} \Delta\mathbf{\Omega}_\alpha = 0; \tag{2.22}$$

2. Since the zeroth-order moment of scattering source should be a scalar, the first-order moment of scattering source should be zero, i.e.
$$v\Sigma_s \sum_{\alpha=1}^{M} \mathbf{e}_\alpha \Delta\mathbf{\Omega}_\alpha \sum_{\alpha'=1}^{M} \psi_{\alpha'} f\left(\alpha,\alpha'\right) \Delta\mathbf{\Omega}_{\alpha'} = 0; \tag{2.23}$$

3. If we assume that the neutron scattering is isotropic $(f=1/4\pi)$, the zeroth-moment of scattering term should be a scalar obtained as
$$\sum_{\alpha=1}^{M} \Delta\mathbf{\Omega}_\alpha \sum_{\alpha'=1}^{M} \psi_{\alpha'} f\left(\alpha,\alpha'\right) \Delta\mathbf{\Omega}_{\alpha'} = \phi; \tag{2.24}$$

4. If the equilibrium distribution function is isotropic (i.e., independent of angular variable), it can be obtained that $\psi^{eq}=\phi/4\pi$ and the second-order moment of equilibrium distribution function can be obtained as
$$\sum_{\alpha=1}^{M} \mathbf{e}_\alpha \mathbf{e}_\alpha \psi_\alpha^{eq} \Delta\mathbf{\Omega}_\alpha = \frac{1}{3} v^2 \phi \mathbf{I}, \tag{2.25}$$

where $\mathbf{I}$ is the unit tensor.

Applying all of these simplification, the neutron conservation equations can be rewritten as
$$\frac{1}{v}\frac{\partial}{\partial t}\phi + \nabla\cdot\mathbf{J} + \Sigma_a\phi = \hat{Q}_\alpha, \tag{2.26}$$
$$\frac{1}{v}\frac{\partial}{\partial t}\mathbf{J} + \frac{1}{3}\nabla\cdot(\phi\mathbf{I}) + \Sigma_t\mathbf{J} = 0. \tag{2.27}$$

The above Eqs. (2.26) and (2.27) are so called P_1 approximation with isotropic scattering assumption and also be known as diffusion theory. The isotropic scattering assumption in this theory is reasonable, since in most conditions, the neutron scattering in nuclear reactor, including inelastic scattering and elastic scattering, can be regarded as isotropic. If treated the neutron scattering as anisotropic process, the scattering cross section could be simply replaced by a Lagrange polynomials and the other processes can be remained [52].

It should be noted that although the diffusion theory is recovered from the NDVBE, the NDVBE is much more accurate than the diffusion theory. On the one hand, the distribution function and temporal derivative are expanded to second-order truncation, while

the source term and spatial derivative are expanded to first-order truncation. On the other hand, Eq. (2.25) applies the assumption that the neutron angular flux is isotropic, which is actually first-order approximation. Due to these approximations, the diffusion solutions will deviate from the NDVBE solutions conceivably and it will be studied in Section 4.

2.2 Finite volume lattice Boltzmann scheme for NDVBE

This part describes the derivation of NFV-LBM by taking the 3D condition as an example and using the finite volume method to process the NDVBE (Eq. (2.2)). The 1D and 2D conditions can be treated as its simplifications. For present NFV-LBM, we divide the computational domain into finite hexahedron control volumes (CVs) and achieve the formulation on a cell-center mesh system. Fig. 1 shows a cell-centered CV with a D3QM lattice, in which the present CV and its boundary are denoted by V_p and ∂V_p, respectively. The CV V_p is surrounded by the adjacent CVs denoted by $V_i\,(i=j,k,l,m,n,o)$ and its vertexes are remarked by A – H. Denoting the interface between V_p and its neighboring V_i by ΔA_{pi}, the boundary ∂V_p can be divided into a collection of interface, i.e. $\partial V_p=\sum_i \Delta A_{pi}$.

According to the definition of V_p, the coordinate of center node p can be determined as

$$\mathbf{r}_p=\sum_{i=A}^{H}\mathbf{r}_i/8, \tag{2.28}$$

in which $\mathbf{r}_i$ with i =A – H represents the coordinate of each vertex.

Averaging the NDVBE (Eq. (2.2)) over the control volume V_p, one obtains

$$\frac{1}{V_p}\int_{V_p}\left(\frac{\partial\psi_\alpha(\mathbf{r},t)}{\partial t}+\mathbf{e}_\alpha\cdot\nabla\psi_\alpha(\mathbf{r},t)\right)dV=\frac{1}{V_p}\int_{V_p}\Pi_\alpha(\psi)dV. \tag{2.29}$$

By using the common practice of widely adopted "lumping" technique [50] in finite volume method (i.e., ψ_α is constant over the CV), the transient term (the first term in Eq. (2.29)) can be simplified as

$$\frac{1}{V_p}\int_{V_p}\frac{\partial\psi_\alpha}{\partial t}dV=\frac{\partial\psi_\alpha(p)}{\partial t}, \tag{2.30}$$

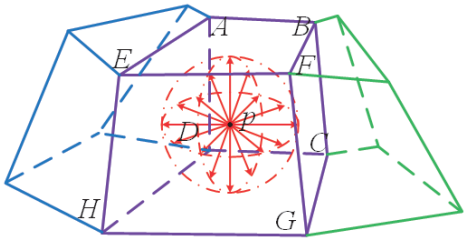

Figure 1: Diagram of 3D cell-centered control volume.

where $\psi_\alpha(p)$ represents the value at centroid p. With the same approximation, the source term (the last term of Eq. (2.29)) can be simplified as

$$\frac{1}{V_p}\int_{V_p}\Pi_\alpha(\psi)dV=\Pi_\alpha(p). \tag{2.31}$$

Thus, the averaging equation (Eq. (2.29)) can be simplified as

$$\frac{\partial\psi_\alpha(p,t)}{\partial t}=\Pi_\alpha(\psi(p,t))-\frac{1}{V_p}\int_{V_p}\mathbf{e}_\alpha\cdot\nabla\psi_\alpha dV. \tag{2.32}$$

The last term of Eq. (2.32) represents the contribution to the balance of ψ_α within V_p due to the microscopic streaming of neutron particle across the interface ∂V_p. Applying the definition $\partial V_p=\sum_i\Delta A_{pi}$ to the advective term, one obtains

$$\int_{V_p}\mathbf{e}_\alpha\cdot\nabla\psi_\alpha dV=\sum_i\psi_{\alpha,pi}\Delta A_{pi}\left(\mathbf{e}_\alpha\cdot\mathbf{n}_{pi}\right), \tag{2.33}$$

in which $\mathbf{n}_{pi}=\mathbf{i}n_{x,pi}+\mathbf{j}n_{y,pi}+\mathbf{k}n_{z,pi}$ is a unit outward normal to the boundary ∂V_p. $\psi_{\alpha,pi}$ represents the value of neutron distribution function at the midpoint of the interface ΔA_{pi}. $\mathbf{e}_\alpha\cdot\mathbf{n}_{pi}$ is the scaled microscopic velocity normal to the interface defined by

$$\mathbf{e}_\alpha\cdot\mathbf{n}_{pi}=\int_{\mathbf{\Omega}_\alpha}v_\alpha\cdot\mathbf{n}_{pi}d\mathbf{\Omega}\Big/\int_{\mathbf{\Omega}_\alpha}d\mathbf{\Omega}. \tag{2.34}$$

Since $\psi_{\alpha,pi}$ belongs to both V_p and V_i, it should satisfy the continuity of angular flux between CVs. To determine it, the step scheme [51] is adopted, which assumes that ψ_α is constant everywhere within the CV and equals to its value at the centroid of upwind control volume. In solving the advection term, the first order upwind scheme can be applied, since the neutron transport process is mainly influenced by its upstream flux and the first order is consistent with the discrete precision of other items. For this reason, the function at the midpoint of interface can be given by

$$\psi_{\alpha,pi}=\begin{cases}\psi_\alpha(p), & \mathbf{e}_\alpha\cdot\mathbf{n}_{pi}>0,\\ \psi_\alpha(i), & \mathbf{e}_\alpha\cdot\mathbf{n}_{pi}<0.\end{cases} \tag{2.35}$$

According to the Eqs. (2.29)-(2.35), the semi-discrete finite volume NDVBE can be modified as

$$\frac{\partial\psi_\alpha(p,t)}{\partial t}=\Pi_\alpha(\psi(p,t))-\frac{1}{V_p}\sum_i\Delta A_{pi}\psi_{\alpha,pi}. \tag{2.36}$$

When considering the neutron transport process in nuclear reactor, the speed of neutron particles can be very large (e.g., the speed of fast neutrons can reach 10^7 cm/s, which involves a high requirement for numerical stability. To ensure the numerical stability and larger time step, the implicit scheme is required.

Discretizing the temporal derivative using the fully implicit backward difference scheme, the implicit finite volume lattice Boltzmann equation can be obtained as

$$\psi_\alpha(p,t)=\psi_\alpha(p,t-\Delta t)+\Delta t\Pi_\alpha(\psi(p,t))-\frac{\Delta t}{V_p}\sum_i \Delta A_{pi}\psi_{\alpha,pi}. \tag{2.37}$$

The implicit finite volume lattice Boltzmann equation can be divided into two processes: Collision:

$$\psi^*_\alpha(p,t)=\psi_\alpha(p,t-\Delta t)+\Delta t\Pi_\alpha(\psi(p,t))-\frac{\Delta t}{V_p}\sum_i \Delta A_{pi}\psi_{\alpha,pi}. \tag{2.38}$$

Streaming:

$$\psi_\alpha(p,t)=\psi^*_\alpha(p,t). \tag{2.39}$$

The above is the establishment for proposed implicit NFV-LBM. Owing to its strong parallel property and simple implementation, the parallel computation of the proposed technique can be easily achieved and can effectively improve the computational efficiency of large engineering computation. Since our NFV-LBM is derived by integrating the NDVBE, and the NDVBE is deduced from the NTE, the current NFV-LBM is actually a NTE solver rather than diffusion theory.

2.3 Boundary condition and implementation

In this part, the treatments of typical boundary conditions are introduced, including vacuum and reflective boundary conditions. The D3QM lattice is taken as an example to illustrate the details of boundary treatments.

Fig. 2 shows the implementation of these two boundaries, in which the facet CDHG lies on the physical boundary of the computational domain. We denote b as the centroid of surface CDHG and p as the centroid of boundary CV. The vacuum and reflective boundary conditions can be considered as a uniform scheme

$$\begin{aligned}&\psi_\alpha(b,t)=\rho_w\psi_{\alpha'}(b,t),\\&\mathbf{n}\cdot\mathbf{e}_\alpha<0,\quad \mathbf{n}\cdot\mathbf{e}_\alpha=-\mathbf{n}\cdot\mathbf{e}_{\alpha'},\end{aligned} \tag{2.40}$$

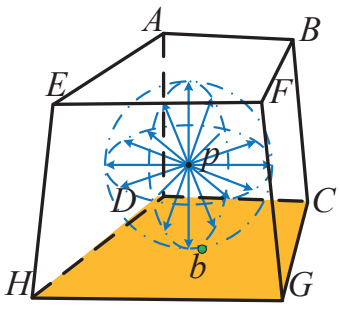

Figure 2: Diagram of numerical implementation of vacuum and reflective boundary conditions.

in which $\mathbf{e}_\alpha$ is the inward lattice speed and $\mathbf{n}$ is the outward normal vector of facet CDHG. $\mathbf{e}_{\alpha'}$ represents the symmetry direction of $\mathbf{e}_\alpha$ related to the physical boundaries and ρ_w is the reflection coefficient defined as

$$\rho_w = \begin{cases} 0, & \text{for vacuum boundary,} \\ 1, & \text{for reflective boundary.} \end{cases} \tag{2.41}$$

After the derivation of NFV-LBM, the proposed technique can be implemented according to the following procedure:

Algorithm 1: Implementation of proposed NFV-LBM.

Input :
Mesh step Δx, time step Δt and lattice speed number n;
The neutron source term Q, cross sections Σ_t, Σ_s, $v\Sigma_f$, etc.;
Total time span $t_{\max}$;
Output:
Neutron flux ϕ;

Initialize the neutron flux ϕ and neutron distribution function ψ;
repeat
$t = t + \Delta t$;
repeat
Calculate the total source term $\Pi_\alpha(\psi)$ according to Eq. (2.3);
Calculate the advection term $\int_{V_p} \mathbf{e}_\alpha \cdot \nabla \psi_\alpha dV$ according to Eqs. (2.33) – (2.35);
Calculate the finite volume lattice Boltzmann equation according to Eqs. (2.40) – (2.41);
Impose the boundary conditions according to Section 2.3;
Calculate the scalar flux ϕ according to Eq. (2.4);
until *convergence*;
Update the neutron distribution function ψ;
until $t = t_{max}$;

3 Verification of NFV-LBM

This part tests two neutron transport cases to verify the accuracy of current NFV-LBM. Solutions of NFV-LBM are compared with those obtained from the literatures.

3.1 1D asymmetric source case

The first case is a 1D transient neutron transport process through a slab initially at a uniform neutron distribution $\psi_0 = 0$ n/(cm·s) (i.e., no particle within the slab at $t = 0^-$) [53].

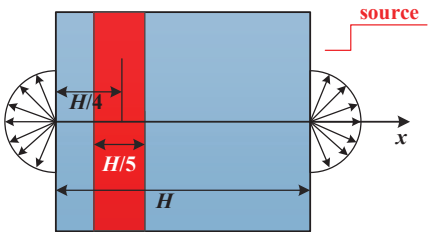

Figure 3: Schematic of 1D transient neutron transport with vacuum boundary.

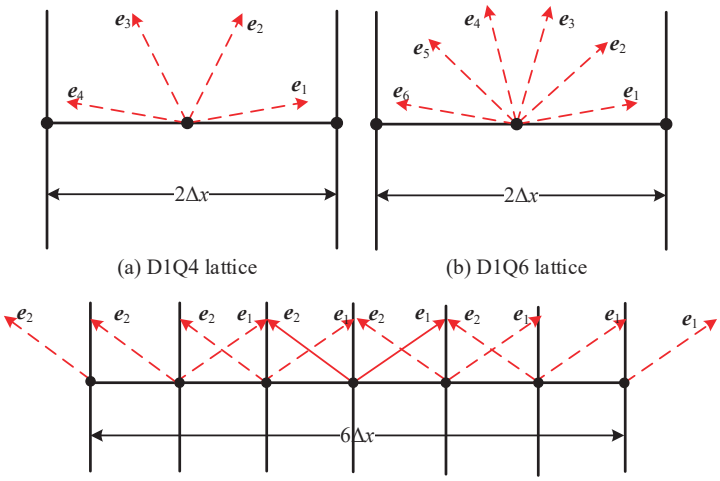

Figure 4: Lattice speeds and lattice configurations for 1D problem.

To verify the applicability of the proposed technique for inhomogeneous and asymmetric source driven condition, the 1D asymmetric source problem is simulated. The unit strength constant source of asymmetric distribution is distributed in the left region of the 1D plane (red) and vacuum boundary is applied to all boundaries, as shown in Fig. 3.

The length of computational domain is $H=5$ cm and the source region is $H/5$ wide in the left region of calculation domain. The macroscopic total cross section Σ_t and the macroscopic scattering cross section Σ_s are taken as 1.0 cm^{-1} and 0.5 cm^{-1}, respectively, which leads to a half-scattering medium. The velocity of neutron particle released from the source region is 1.0 cm/s and the neutron particle source turns on at $t=0^+$ s and remains on for the entire simulation.

In simulation, the 101 mesh configuration is adopted and the D1Q2, D1Q4 and D1Q6 lattices are applied. Fig. 4 shows the lattice speeds for D1Q2, D1Q4 and D1Q6 lattice models. The lattice configurations for inner nodes and vacuum boundary nodes are also represented in this schematic. From Fig. 4(a) and 4(b), one can find that the discrete velocities are only distributed in the upper semicircle, which is a numerical simplification

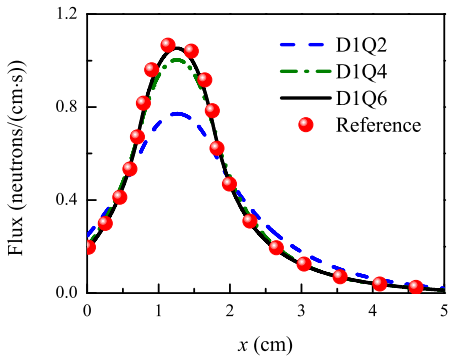

Figure 5: Comparison between NFV-LBM and Ref. [53] with different lattices.

since the velocity space is symmetric. For the vacuum boundary, the inward distribution functions are equal to 0, thus there are only outward distribution functions on the boundary nodes, as shown in Fig. 4(c). Besides, 2D and 3D discrete velocity models can be obtained similarly.

Fig. 5 shows the comparisons between the NFV-LBM solutions and those obtained from the literature [53] in steady state. The reference solutions for 1D asymmetric source problem are obtained from the direct transport solution with 500 meshes and 50 discrete directions, and the tolerance for convergence of iteration is set to 10^{-6}. These reference solutions can be in good agreements with the solutions of standard integral equation and numerical integration solutions [54], which are regarded as the analytical exact solutions. It can be seen that the NFV-LBM solutions are gradually close to the reference value as the number of lattice speed increases. The D1Q6 solution is in good agreement with the transport solution whilst the D1Q2 and D1Q4 results obviously deviate from them. Actually, when the number of lattice speed higher than 6, the steady-state solution will never change, namely reaching the lattice speed independence.

3.2 2D asymmetric source case

The second case is a 2D square slab with the symmetric source distributed in the center of slab (red) [55], as shown in Fig. 6. This condition is a very common situation in nuclear engineering field since the configuration of fuel assembly is a non-uniform source surrounded by moderator. The source strength is taken as $q=1.0$ n/(cm^2·s) and the vacuum boundary is adopted to all the boundaries.

The width of square slab is set as $H=2.0$ cm and the source width is set as $H_s=1.04$ cm. The macroscopic total cross section Σ_t is set as 1.0 cm^{-1} while the albedo $c=\Sigma_s/\Sigma_t$ is taken as 0, 0.5 and 0.75, which make the computing domain from the pure absorbing medium to a strongly scattering medium. In simulating this case, 101×101 mesh configuration is adopted. To illustrate the flexibility and adaptability on grid of this technique, both the quadrilateral and triangular meshes are adopted to simulate the 2D neutron transport

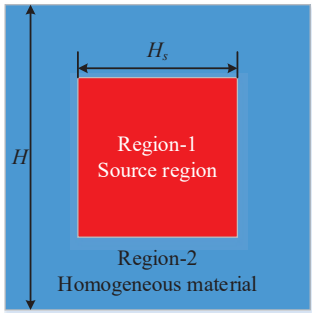

Figure 6: Schematic of 2D neutron transport problem.

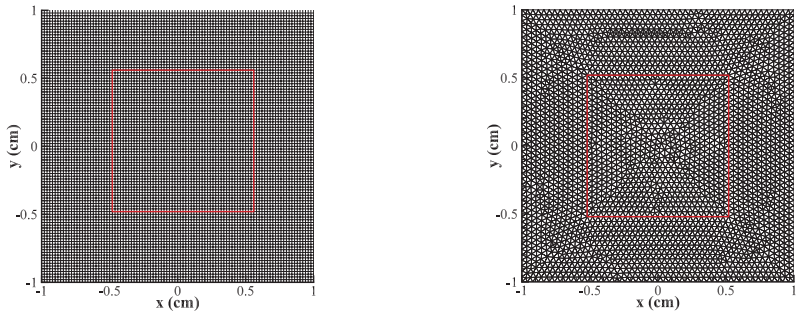

Figure 7: Mesh configurations for quadrilateral (left) and triangular (right) meshes.

problem. The mesh configurations for quadrilateral (left) and triangular (right) meshes are shown in Fig. 7, in which the red squares represent the interfaces between source regions and non-source regions.

Solutions obtained from quadrilateral and triangular meshes are compared with each other by using the same lattice speed model, as shown in Fig. 8. It can be seen that, at different albedos, all triangular mesh solutions are in good agreements with those of quadrilateral mesh, indicating that the proposed technique can be applied to both quadrilateral and triangular meshes flexibly.

For this case is a 2D case, the D2QM and D3QM lattice models are all considered, in which the lattice speeds included azimuth and polar discretization, since the polar angular is anisotropic actually. Different lattice speed configurations are applied to analyze the effect of M on the accuracy of the NFV-LBM. Steady-state profiles of neutron distribution will be reached after sufficiently long time. The steady-state neutron distributions along the diagonal line with different lattices are shown in Fig. 9. Among them, the D3QM models are achieved on the basis of D2Q12 model by increasing lattice speed of polar angle.

In choosing the number of discrete lattice speed (M), the rotation invariance needs to be guaranteed firstly. Fig. 9 shows the numerical solutions in different albedos: (a)–(b) $c=0$, (c)–(d) $c=0.5$ and (e)–(f) $c=0.75$. As shown in Fig. 9, with the increase of discrete

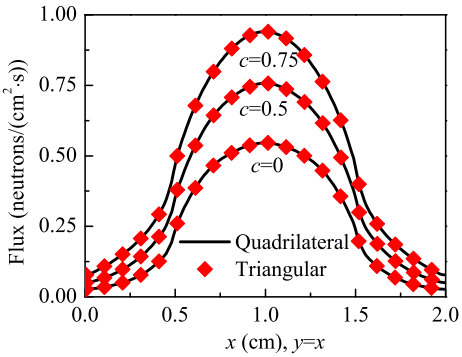

Figure 8: Comparisons between quadrilateral and triangular mesh based solutions.

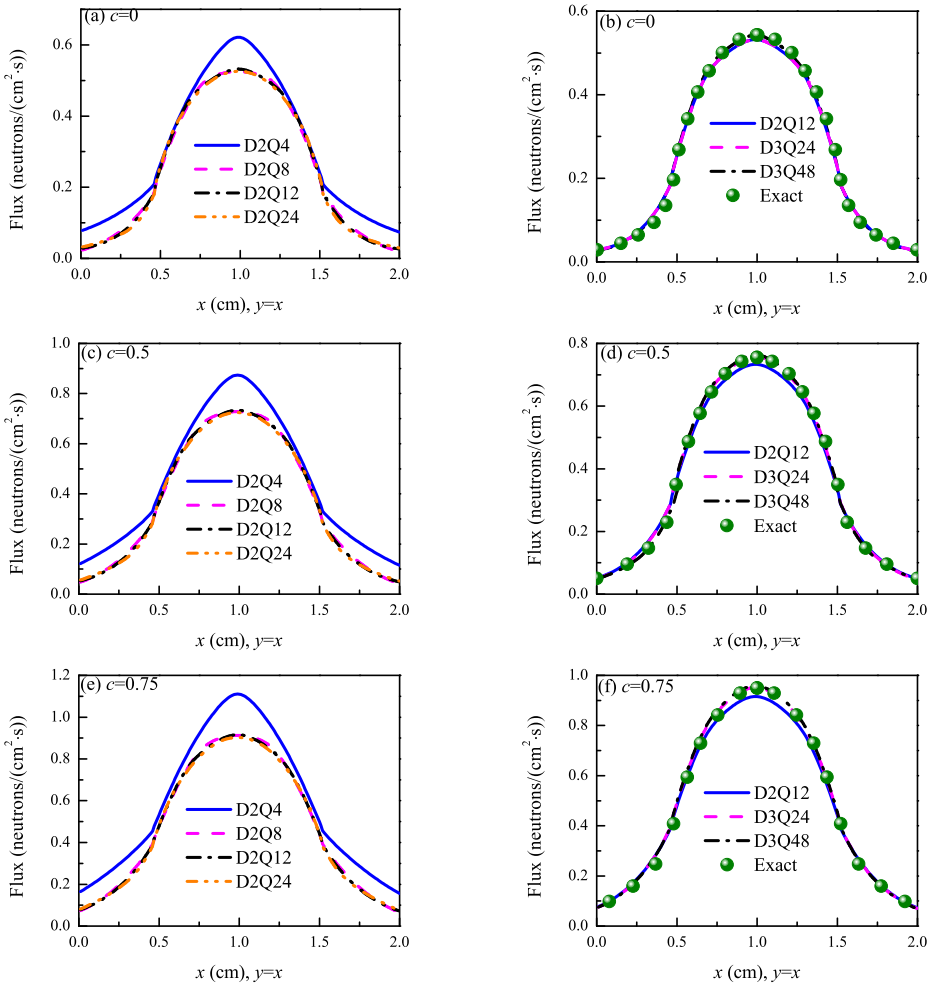

Figure 9: Neutron distribution in different albedos and lattices.

lattice speed, the NFV-LBM solutions will gradually reach lattice speed independent and close to the exact solutions [55], and it can be seen that with the same plane lattice speed allocation, the D3QM model can be more accurate than D2QM model. When considering the azimuth angle only, the NFV-LBM solutions will deviate the exact solutions, and even if the 2D problem is solved, the polar angle discretization should still be considered. These two cases indicate that the proposed NFV-LBM can be applied to simulate the neutron transport problems and its accuracy will be strongly affected by lattice model.

From all these two verifications, one can find that different lattice models can lead to different accuracies of computational solutions. To ensure the precision of transport theory, the lattice speed independence should be satisfied, and for rotation invariance, the symmetry of the lattice speeds needs to be guaranteed firstly. In the present work, some lattice models satisfying the lattice speed independence are given, and for most problems, these lattice models can be applied directly. Besides, for some unique problems, the independent lattice models can be obtained with the same process.

4 Comparison between NFV-LBM and diffusion theory

Section 2.1 has proved from the mathematical point of view that the diffusion theory is a lower-order approximation of NDVBE. In this part, we simulate two neutron propagation processes to compare the NDVBE and diffusion theory from spatial scale, temporal scale and medium property.

4.1 Analysis of spatial and temporal scales

In this case, we analyze the neutron transfer process using both NFV-LBM and diffusion theory to study the effects of spatial and temporal scales on these two theoretical solutions. This case is a 1D problem in which the 1D plane is divided into two part, including source region (red) and homogeneous material (blue), as shown in Fig. 10.

The computing domain is initially at a uniform neutron distribution $\psi_0 = 0$ n/(cm·s). All the boundaries are vacuum boundaries and the internal assembly interface is continuous. The neutron particle can exchange between source region and homogeneous material but cannot enter from the surrounding. The macroscopic total cross section is set as $\Sigma_t = 1.0$ cm^{-1}, and the macroscopic scattering cross sections is set as $\Sigma_s = 0.5$ cm^{-1},

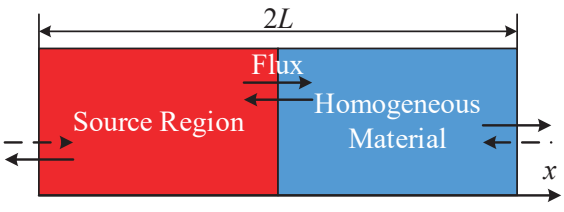

Figure 10: Geometric and physical conditions for 1D case with different spatial scale.

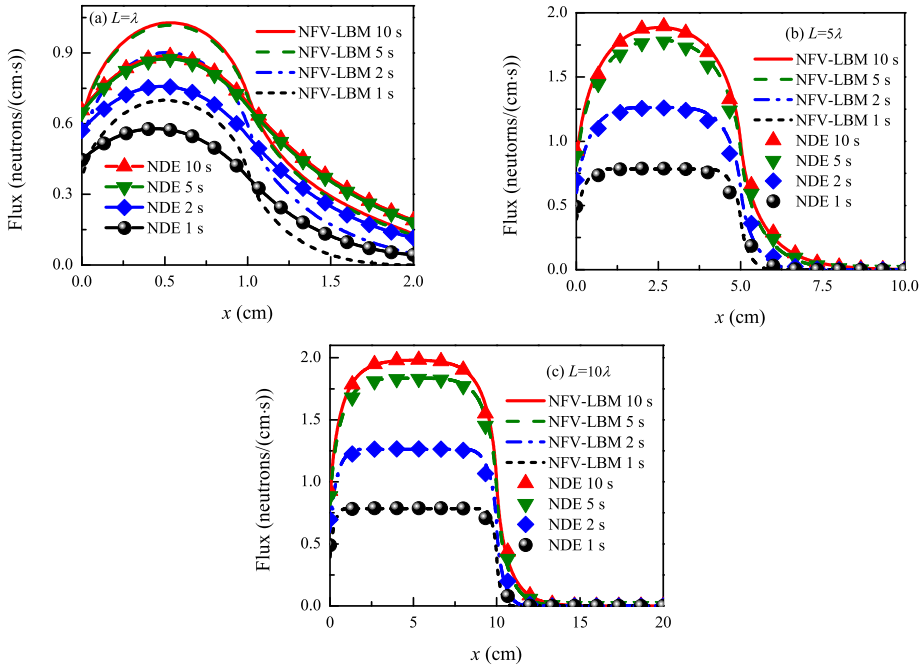

Figure 11: Comparisons of NFV-LBM and NDE solutions in different spatial scales.

which leads to a half-scattering medium. The neutron velocity released from the medium is set as $v=1.0$ cm/s.

It is easy to determine that the mean free path (mfp) of this medium is $\lambda=1/\Sigma_t=1$ cm and the mean free time (mft) for neutron particle in this medium is $\lambda/v=1$ s. Thus, to analyze the influence of spatial scale, the length of 1D plane is set as (a) $L=\lambda=1$ mfp, (b) $L=5\lambda=5$ mfp and (c) $L=10\lambda=10$ mfp and the transient solutions are tested at 1 mft, 2 mft, 5 mft and 10 mft. As concluded in Section 3.1, the D1Q6 lattice and 101 mesh configuration are adopted.

Fig. 11 shows the comparisons between NFV-LBM and diffusion solutions, in which the transient solutions are compared in all three spatial scales. It can be seen that for the case (a), the diffusion theory will strongly underestimate the neutron flux distribution level and overestimate that in non-source region. Since in the diffusion theory, the angle-dependent of the neutron flux is neglected, and the diffusion function is supposed to be the governing mechanism of neutron propagation, the neutron diffusion solutions smooth out the neutron flux especially when considering the smaller medium. For larger spatial scales (cases (b) and (c)), solutions of diffusion theory close to NFV-LBM solution gradually along the increase of spatial scale. The diffusion solutions for case (b) slightly deviate the NFV-LBM solutions at the beginning of a short period of time and agree well with NFV-LBM solutions at longer temporal scale, whilst the diffusion solutions in case (c) always agree well with the NFV-LBM solutions. Thus, the diffusion solutions will

close to the NFV-LBM solution with the increases of spatial and temporal scales. These conclusions are consistent with the results of neutron transport theory, indicating that the NFV-LBM is much more accurate than diffusion theory and has similar results with neutron transport theory.

4.2 Analysis of physical property

This case is set to study the effect of neutron property. In this case, a 1D symmetric source problem is studied and the geometry is shown in Fig. 12, in which the source region (red) is surrounded by two homogeneous materials (blue), the vacuum boundary is applied to all the physical boundaries and the internal assembly interface is continuous. The macroscopic total cross section is Σ_t=1.0 cm^{-1} thus the mean free path of neutron particle in this medium is $\lambda=1$ cm. The length of 1D slab is $H=5$ mfp while the length of the source term in the centroid of medium is $H_s=H/2$. Similarly, the D1Q6 lattice and 101 mesh configuration are adopted.

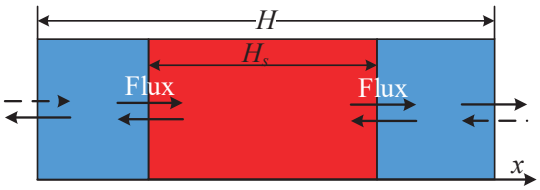

Figure 12: Schematic of 1D symmetric source problem.

To study the influence of physical property, we simulate the neutron transfer with different albedos, including c=1, c=0.9, c=0.5, c=0.1 and c=0, which make the computing domain from a pure scattering medium to a pure absorbing medium. The steady-state neutron particle distribution from NFV-LBM and diffusion theory are compared with each other and the relative errors are also calculated. The relative error is defined as

$$\frac{\left|\phi_{NFV-LBM}-\phi_{diffusion}\right|}{\phi_{NFV-LBM}}\times 100\%,$$

to characterize the degree of the diffusion solutions deviating from the NFV-LBM solutions, in which $\phi_{NFV-LBM}$ and $\phi_{diffusion}$ represent the solutions of NFV-LBM and diffusion theory, respectively.

Fig. 13 shows the normalized neutron fluxes and their relative errors in different albedos: (a)–(b) $c=1.0$, (c)–(d) $c=0.9$, (e)–(f) $c=0.5$, (g)–(h) $c=0.1$ and (i)–(j) $c=0$. As shown in Fig. 13, the diffusion theory always underestimates the neutron distribution in source region and overestimate that in non-source region since the diffusion theory always make the neutron distribution smooth. Besides, owing to the mutation of neutron particle source, the relative error will occur a sharp change in the assembly interface.

For a clearer explanation, we describe the averaging error for all albedos in Fig. 14, in which the black solid line is the trend line of the average error's increase. From Fig. 14,

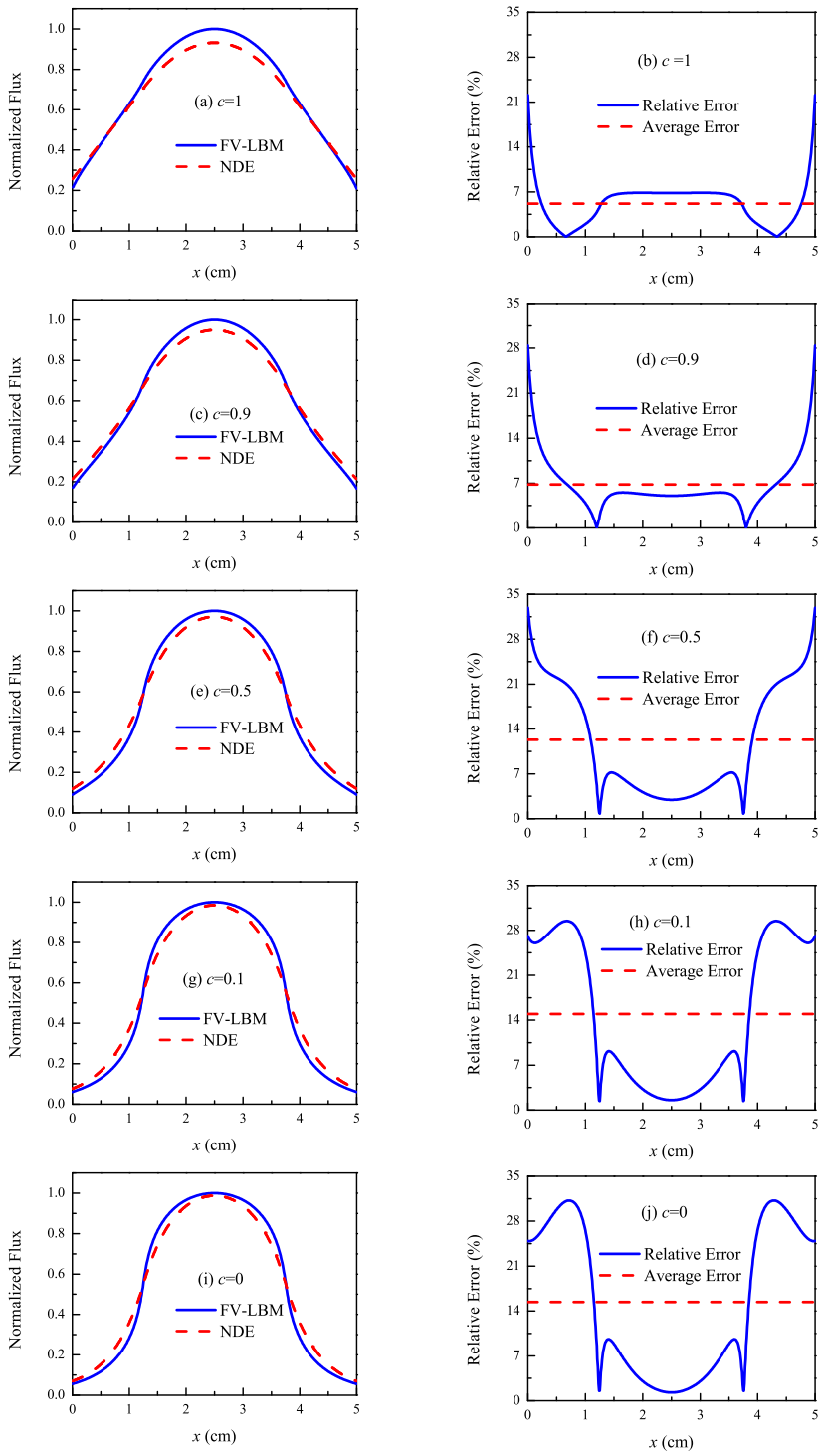

Figure 13: Comparison between NFV-LBM and NDE solutions and its relative error.

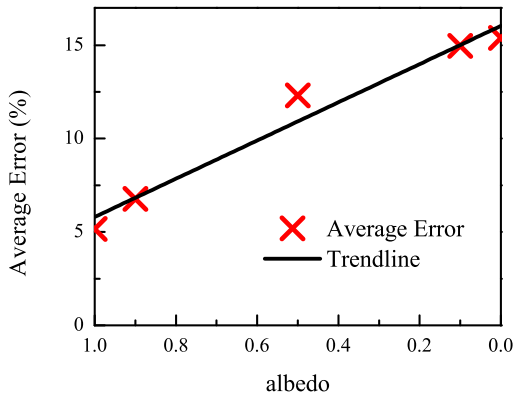

Figure 14: Averaging errors for different albedos.

one can obviously conclude that the average error increases with the decrease of albedo, since the diffusion theory will be more reasonable for high scattering medium. Because the accuracy of proposed NFV-LBM was verified at the previous section, this case indicates that the diffusion theory will close to both the NFV-LBM and transport solutions with the increase of albedo.

5 Conclusion

This paper presents an implicit NFV-LBM for solving the NDVBE and the relation between NDVBE and diffusion theory is studied. The NFV-LBM is established by integrating the NDVBE, which is deduced from the NTE and the non-linear collision term for NDVBE is omitted owing to neglecting the inter-particle collision. Numerical solutions show that the NFV-LBM can simulate the neutron transport problem accurately and flexibly, indicating that the NDVBE has the same accuracy of NTE. To study the relationship between the NFV-LBM and diffusion theory, both the multi-scale expansion and the numerical simulations are applied. Results show that the diffusion theory can be recovered from NDVBE via lower-order expansion and the diffusion solution will deviate the NFV-LBM solution in small spatial scale and short temporal scale. Besides, the strongly absorbing medium will lead to a large derivation between NFV-LBM and diffusion solutions. This paper may provide some alternative perspectives for solving the NTE and some new ideas for studying the relationship between the NTE and other NTE approximations.

Acknowledgments

This work is supported by the State Key Program of National Natural Science of China under Grant No. 51436009.

References

[1] J. J. Duderstadt, L. J. Hamilton, Nuclear Reactor Analysis, John Wiley, New York, 1976.
[2] B. Davison, J. B. Sykes, Neutron transport theory, Clarendon Press, Oxford, 1957.
[3] Y. Oka, Nuclear Reactor Design, Springer, Tokyo, 2014.
[4] R. F. Barth, A critical assessment of boron neutron capture therapy: an overview, J. Neuro-Oncol., 62 (2003), 1–5.
[5] A. M. Mirza, S. Iqbal, F. Rahman, A spatially adaptive grid-refinement approach for the finite element solution of the even-parity Boltzmann transport equation, Ann. Nucl. Energy, 34 (2007), 600–613.
[6] E. E. Lewis, W. F. Miller, Computational Methods of Neutron Transport, John Wiley & Sons, New York, 1984.
[7] K. Wang, Z. G. Li, D. She, J. G. Liang, Q. Xu, Y. S. Qiu, J. K. Yu, J. L. Sun, X. Fan, G. L. Yu, RMC–A Monte Carlo code for reactor core analysis, Ann. Nucl. Energy, 82 (2015), 121–129.
[8] Y. S. Qiu, M. Aufiero, K. Wang, M. Fratoni, Development of sensitivity analysis capabilities of generalized responses to nuclear data in Monte Carlo code RMC, Ann. Nucl. Energy, 97 (2016), 142–152.
[9] Z. Y. Wu, Q. Zhang, H. Abdel-Khalik, Hybrid Monte Carlo-deterministic methods for reactor analysis, Nucl. Technol., 180 (2012), 372–382.
[10] J. C. Chai, S. V. Patankar, H. S. Lee, Evaluation of spatial differencing practices for the discrete-ordinates method, J. Thermophys. Heat Tr., 8 (1994), 140–144.
[11] M. T. Calef, E. D. Fichtl, J. S. Warsa, M. Berndt, N. N. Carlson, Nonlinear Krylov acceleration applied to a discrete ordinates formulation of the k-eigenvalue problem, J. Comput. Phys., 238 (2013), 188–209.
[12] J. K. Fletcher, The solution of the multigroup neutron transport equation using spherical harmonics, Nucl. Sci. Eng., 84 (1983), 33–46.
[13] Q. C. Chen, H. C. Wu, L. Z. Cao, Auto MOC—A 2D neutron transport code for arbitrary geometry based on the method of characteristics and customization of AutoCAD, Nucl. Eng. Des., 238 (2008), 2828–2833.
[14] Z. Y. Liu, H. C. Wu, L. Z. Cao, Q. C. Chen, Y. Z. Li, A new three-dimensional method of characteristics for the neutron transport calculation, Ann. Nucl. Energy, 38 (2011), 447–454.
[15] A. Zhu, M. Jarrett, Y. L. Xu, B. Kochunas, E. Larsen, T. Downar, An optimally diffusive Coarse Mesh Finite Difference method to accelerate neutron transport calculations, Ann. Nucl. Energy, 95 (2016), 116–124.
[16] R. A. Forster, T. N. K. Godfrey, MCNP - a general Monte Carlo code for neutron and photon transport, Springer, Berlin, 1985.
[17] D. She, Y. X. Liu, K. Wang, G. L. Yu, B. Forget, P. K. Romano, K. Smith, Development of burnup methods and capabilities in Monte Carlo code RMC, Ann. Nucl. Energy, 51 (2013), 289–294.
[18] F. J. Higuera, S. Succi, Simulating the flow around a circular cylinder with a lattice Boltzmann equation, Europhys. Lett., 8 (1989), 517.
[19] S. Y. Chen, G. D. Doolen, Lattice Boltzmann method for fluid flows, Ann. Rev. Fluid Mech., 30 (1998), 329–364.
[20] X. Y. He, L. S. Luo, Theory of the lattice Boltzmann method: From the Boltzmann equation to the lattice Boltzmann equation, Phys. Rev. E, 56 (1997), 6811.
[21] P. Wang, Y. H. Zhang, Z. L. Guo, Numerical study of three-dimensional natural convection in a cubical cavity at high Rayleigh numbers, Int. J. Heat Mass Tran., 113 (2017), 217–228.

[22] Z. L. Guo, C. Shu, Lattice Boltzmann method and its applications in engineering, World Scientific, 2013.
[23] Q. Li, Y. L. He, G. H. Tang, W. Q. Tao, Improved axisymmetric lattice Boltzmann scheme, Phys. Rev. E, 81 (2010), 056707.
[24] X. Y. He, S. Y. Chen, G. D. Doolen, A novel thermal model for the lattice Boltzmann method in incompressible limit, J. Comput. Phys., 146 (1998), 282–300.
[25] Q. J. Kang, D. X. Zhang, S. Y. Chen, X. Y. He, Lattice Boltzmann simulation of chemical dissolution in porous media, Phys. Rev. E, 65 (2002), 036318.
[26] K. Xu, X. Y. He, Lattice Boltzmann method and gas-kinetic BGK scheme in the low-Mach number viscous flow simulations, J. Comput. Phys., 190 (2003), 100–117.
[27] Y. M. Xuan, Q. Li, M. Ye, Investigations of convective heat transfer in ferrofluid microflows using lattice-Boltzmann approach, Int. J. Therm. Sci., 46 (2007), 105–111.
[28] G. D. Prisco, X. W. Shan, Mass Transport/Diffusion and Surface Reaction Process with Lattice Boltzmann, Commun. Comput. Phys., 9 (2011), 1362–1374.
[29] F. Chen, A. G. Xu, G. C. Zhang, Viscosity, heat conductivity, and Prandtl number effects in the Rayleigh-Taylor Instability, Front. Phys., 11 (2016), 114703.
[30] Y. Ma, S. K. Dong, H. P. Tan, Lattice Boltzmann method for one-dimensional radiation transfer, Phys. Rev. E, 84 (2011), 016704.
[31] S. C. Mishra, R. R. Vernekar, Analysis of transport of collimated radiation in a participating media using the lattice Boltzmann method, J. Quant. Spectrosc. Ra., 113 (2012), 2088–2099.
[32] X. W. Shan, H. D. Chen, Lattice Boltzmann model for simulating flows with multiple phases and components, Phys. Rev. E, 47 (1993), 1815–1819.
[33] L. Zhang, Q. J. Kang, C. Li, J. Yao, Simulation of Flow in Multi-Scale Porous Media Using the Lattice Boltzmann Method on Quadtree Grids, Commun. Comput. Phys., 19 (2016), 998–1014.
[34] A. D'Orazio, S. Succi, Simulating two-dimensional thermal channel flows by means of a lattice Boltzmann method with new boundary conditions, Future Gener. Comp. Sy., 20 (2004), 935–944.
[35] Z. W. Tian, C. Zou, Z. H. Liu, Z. L. Guo, H. J. Liu, C. G. Zheng, Lattice Boltzmann method in simulation of thermal micro-flow with temperature jump, Int. J. Mod. Phys. C, 17 (2006), 603–614.
[36] N. Prasianakis, S. Ansumali, Microflow Simulations via the Lattice Boltzmann Method, Commun. Comput. Phys., 9 (2011), 1128–1136.
[37] D. O. Martínez, S. Y. Chen, W. H. Matthaeus, Lattice Boltzmann magnetohydrodynamics, Phys. Plasmas, 1 (1994), 1850–1867.
[38] A. Nabovati, D. P. Sellan, C. H. Amon, On the lattice Boltzmann method for phonon transport, J. Comput. Phys., 230 (2011), 5864–5876.
[39] Y. Y. Guo, M. R. Wang, Lattice Boltzmann modeling of phonon transport, J. Comput. Phys., 2016 (2016), 1–15.
[40] H. Bindra, D. Patil, Radiative or neutron transport modeling using a lattice Boltzmann equation framework, Phys. Rev. E, 86 (2012), 016706.
[41] A. Gairola, H. Bindra, Lattice Boltzmann method for solving non-equilibrium radiative transport problems, Ann. Nucl. Energy, 99 (2016), 151–156.
[42] R. Mcculloch, H. Bindra, Coupled radiative and conjugate heat transfer in participating media using lattice Boltzmann methods, Comput. Fluids, 124 (2016), 261–269.
[43] O. Malaspinas, B. Chopard, J. Latt, General regularized boundary condition for multi-speed lattice Boltzmann models, Comput. Fluids, 49 (2011), 29–35.

[44] R. Mason, A multi-speed compressible lattice-Boltzmann model, J. Stat. Phys., 107 (2002), 385–400.
[45] D. Lycett-Brown, I. Karlin, K. Luo, Droplet Collision Simulation by a Multi-Speed Lattice Boltzmann Method, Commun. Comput. Phys., 9 (2011), 1219–1234.
[46] S. Succi, A. Zarghami, S. Ubertini, Finite volume formulation of thermal lattice Boltzmann method, Int. J. Numer. Method. H., 24 (2014), 270–289.
[47] Y. T. Chew, C. Shu, Y. Peng, On Implementation of Boundary Conditions in the Application of Finite Volume Lattice Boltzmann Method, J. Stat. Phys., 107 (2002), 539–556.
[48] A. Zarghami, M. J. Maghrebi, J. Ghasemi, S. Ubertini, Lattice Boltzmann Finite Volume Formulation with Improved Stability, Commun. Comput. Phys., 12 (2012), 42–64.
[49] F. Nannelli, S. Succi, The lattice Boltzmann equation on irregular lattices, J. Stat. Phys., 68 (1992), 401–407.
[50] K. W. Morton, Numerical solution of convection-diffusion problems, Chapman & Hall, London, 1996.
[51] P. J. Coelho, Advances in the discrete ordinates and finite volume methods for the solution of radiative heat transfer problems in participating media, J. Quant. Spectrosc. Ra., 145 (2014), 121–146.
[52] A. Hébert, Applied reactor physics, Presses inter Polytechnique, 2nd Edition, 2009.
[53] P. Picca, R. Furfaro, A hybrid method for the solution of linear Boltzmann equation, Ann. Nucl. Energy, 72 (2014), 214–236.
[54] K. R. Olson, D. L. Henderson, Numerical benchmark solutions for time-dependent neutral particle transport in one-dimensional homogeneous media using integral transport, Ann. Nucl. Energy, 31 (2004), 1495–1537.
[55] R. W. Tsai, S. K. Loyalka, A numerical method for solving the integral equation of neutron transport: III, Nucl. Sci. Eng., 61 (1976), 536–540.